Applied Catalysis B: Environmental 207 (2017) 376–384

Contents lists available at ScienceDirect

Applied Catalysis B: Environmental

journal homepage: www.elsevier.com/locate/apcatb

Could NO_x be released during mineralization of pollutants containing nitrogen by hydroxyl radical? Ascertaining the release of N-volatile species

Sergi Garcia-Segura[a,*], Ehab Mostafa[a,b], Helmut Baltruschat[a,*]

[a] Institute of Physical and Theoretical Chemistry, University of Bonn, D-53117 Bonn, Germany
[b] Chemistry Department, Faculty of Science, Mansoura University, 35516 Mansoura, Egypt

ARTICLE INFO

Article history:
Received 2 December 2016
Received in revised form 20 January 2017
Accepted 11 February 2017
Available online 14 February 2017

Keywords:
Differential electrochemical mass spectroscopy (DEMS)
Boron-doped diamond anodes (BDD)
Electrochemical oxidation (EO)
Water treatment
Contaminants of emerging concern

ABSTRACT

Advanced oxidation processes emerged as highly promising water treatment technologies for the abatement of organic pollutants in waters. The treatment of N-containing aromatic pollutants such as amines and nitro-derivatives is of great relevance due to their carcinogenicity. However, one of the major questions is the possible release of NO_x species from the oxidation of these pollutants by •OH. The evolution of these hazardous NO_x during the water treatments by •OH has been suggested to explain the loss of nitrogen during the mass balances, but unfortunately this hypothesis has not been demonstrated experimentally. In this work, the release of NO_x has been ascertained and the overall current efficiency of conversion of N-containing pollutants to CO_2 and NO_x was estimated semi-quantitatively using differential electrochemistry mass spectroscopy (DEMS) during electrochemical advanced oxidation process with boron-doped diamond (BDD) anodes. Moreover, the relationship between the distributions of N-volatile species with the nitrogenized functional group of each pollutant has been highlighted.

1. Introduction

Water recycling is one of the greatest challenges of this century. The water pollution is a major concern due to the direct affectation of the environment. It has been demonstrated that the presence of persistent organic pollutants and contaminants of emerging concern in water effluents on the range of ng dm^{-3} up to mg dm^{-3} could present hazardous effects such as carcinogenicity or toxicity among other undesirable side-effects [1–3]. Conventional water treatment technologies cannot remove efficiently these pollutants from aqueous bodies, thus the development of novel emerging technologies is crucial [4,5]. In this context, the advanced oxidation processes (AOPs) have been considered as highly promising technologies on the abatement of these highly recalcitrant organic pollutants. The AOPs fundamentals consist of generating *in situ* reactive oxygen species (ROS) like the strong oxidant hydroxyl radical (•OH) with E° = 2.8 V vs. SHE, which is capable to completely mineralize organic pollutants to CO_2 and water [4–7]. In this context, several papers have reported the efficient abatement of organic pollutants by photocatalysis [8,9], ozonation [10,11], Fenton process [12,13], electro-Fenton [14,15] or electrochemical oxidation (EO) [16–18].

The mineralization of nitrogen-containing pollutants yields N-species apart from the expected CO_2 and water. Generally, the main considered N-species are NH_4^+, NO_2^- and NO_3^-. Nonetheless, taking into account these species, the nitrogen mass balance is in general terms incomplete [12–18]. Furthermore, when the total nitrogen in solution is quantified and followed versus treatment time, a loss of the nitrogen in the solution is evidenced [18]. In the presence of high concentrations of chloride anion where active chlorine species can be released, the loss of nitrogen can be related to the formation of chloramines and the loss of nitrogen as N_2 [16]. However, the general hypothesis to justify this trend when hydroxyl radical is the main oxidant involved in the mineralization process is the formation of N-volatile species such NO_x species. Unfortunately, the identification of these species has not been previously reported in literature. Noteworthy is that to better understand the catalytic pollutants mineralization by •OH, the clarification of this point is unavoidable and is of major relevance since these volatile species are considered noxious and hazardous.

The research undertaken in this work aimed at identifying the formation of N-volatile species from their oxidation mediated by •OH to gain a better understanding of the oxidation reactions of ROS with organic pollutants. Four N-containing organic compounds

* Corresponding authors.
E-mail addresses: sergigarcia@ub.edu (S. Garcia-Segura), baltruschat@uni-bonn.de (H. Baltruschat).

http://dx.doi.org/10.1016/j.apcatb.2017.02.046
0926-3373/

with different functional groups were selected as model pollutants and treated by EO using boron-doped diamond (BDD) anode. In EO, •OH is electrogenerated on the surface of oxygen terminated BDD anode from water oxidation Reaction (1), which could be obtained at high applied potentials [4,19]. Thus, the electrogenerated •OH is considered as the main responsible of the indirect oxidation of pollutants, although direct charge transfer processes could be also feasible [4,20]. For instance, in some cases (e.g. oxidation of CO and hexafluoroisopropanol) it has been shown that the reaction is initialized by an attack of the •OH followed by an additional direct electron transfer [21,22]. It should be noted that other oxidant species such ozone, hydrogen peroxide or hydroperoxil radical could be electrogenerated in low concentration during EO, although due to their minor contribution to the overall oxidation of organics in EO have not been considered.

$$H_2O \rightarrow {}^{\bullet}OH + H^+ + e^- \quad (1)$$

To identify the N-volatile species, the EO was carried out using Differential Electrochemical Mass Spectroscopy (DEMS). This analytic technique allows the on-line and simultaneous detection of volatile reaction products after their formation during cyclic voltammetry assays [22,24]. Thereby, during the potential sweep, the faradaic current and the ionic currents of $m/z = 44$ (CO_2), $m/z = 46$ (NO_2) and $m/z = 30$ (NO) were simultaneously recorded during pollutants oxidation allowing the identification of these N-volatile species that have not been reported before in literature. Furthermore, the distribution of these species in function of the nitrogen functional group is discussed.

2. Experimental

2.1. Chemicals

Benzoic acid (>99.5% purity), 4-aminobenzoic acid (>99% purity), 4-(methylamino)benzoic acid (97% purity) and 4-(dimethylamino)benzoic acid (98% purity) were purchased from Sigma-Aldrich, while 4-nitrobenzoic acid (>99% purity) was acquired from Acros organics. The characteristics and chemical structures of these compounds are summarized in Table 1. Sodium perchlorate monohydrate (>99% purity) used as supporting electrolyte was purchased from Fluka analytical. Sodium hydroxide and perchloric acid were used to adjust the pH and were of analytical grade supplied by Sigma-Aldrich. All solutions were prepared with Millipore-Milli Q high-purity water of resistivity >18 MΩ cm at 25 °C (Schwalbach, Germany). The solutions were deareated with highly pure argon (99.999%).

2.2. Electrolytic system

The solutions pH was adjusted and determined by using a Knick 766 Calimatic pH-meter. The electrolysis were conducted in a dual thin layer flow cell as depicted in the scheme of Fig. 1. The solution first flows from the inlet into the thin layer compartment containing the BDD working electrode. There, the organic pollutants are oxidized by the •OH electrogenerated *in-situ*. The solution then flows through six small capillaries into a second compartment below where the volatile species are removed from the aqueous solution through a porous Teflon membrane to the vacuum inlet of the mass spectrometer (Balzers quadrupole QMG-422) [25,22]. Finally, the solution leaves this compartment through the outlet at the center closing the hydraulic circuit.

The geometric surface area of 0.28 cm^2 of the BDD electrode was defined by a thin Teflon o-ring (Gore-Tex®) with an inner diameter of 6 mm, whilst the thickness of the thin electrolyte layer of 200 μm was defined by the thickness of this former Teflon o-ring. The flow rate of the solutions was adjusted to 5 μL s^{-1} by a peristaltic pump (Perimax-Spectec®) positioned at the outlet of the DEMS cell [23]. A reversible hydrogen electrode (RHE) placed at the inlet (see Fig. 1) was used as a reference electrode, whilst Pt wires were used as counter electrodes. In order to optimize the current distribution in the dual thin layer cell as well as diminishing the *iR*-drop resistance, these two Pt wire electrodes were placed at the inlet and outlet of the cell and connected via a resistance of 1100 Ω and 100 Ω, respectively [21–25]. Voltammetric analyses were conducted at 25 °C with a home-built potentiostat and function generator and the data were collected using a LabView software (National Instruments GmbH) at scan rate of 10 mV s^{-1} from 0 up to 3.0 V vs RHE. The solutions were purged with high purity Ar gas for 30 min and the Ar saturation maintained during the experimental runs. In a separate three electrode cell employing BDD as a working electrode, RHE as a reference and Pt sheet as a counter electrode, the BDD anode was cleaned before conducting each experiment by several voltammetric cycles in 0.5 M H_2SO_4 from 0 up to 3 V, and rinsed afterwards with Millipore-Milli Q high-purity water.

On the other hand the current efficiency (*CE*) can be calculated according to expression (4) [23]:

$$CE = \frac{Q_F^*}{Q_F} \quad (4)$$

where, Q_F is the total faradaic charge and Q_F^* is the partial faradaic charge corresponding to the formation of the *i* volatile species, which is determined from Eq. (5):

$$Q_F^* = \frac{zQ_i}{K_i^*} \quad (5)$$

where, Q_i is the ionic charge of the *i* volatile species, *z* is the number of electrons involved in the generation of each *i* volatile species and K_i^* is the calibration constant for each species. The contribution on CO_2 signal due to the corrosion of BDD obtained from the blank was subtracted from the overall CO_2 ion current. K^* for CO_2 was experimentally determined from the oxidation of adsorbed CO on polycrystalline Pt: CO was adsorbed at a constant electrode potential of 0.06 V vs. RHE by replacing the supporting electrolyte with a CO saturated 0.5 M H_2SO_4 electrolyte (ca. 10^{-3} mol L^{-1}). After the formation of a CO monolayer, the solution was exchanged with pure supporting electrolyte under potential control ($E = 0.06$ V vs. RHE), in order to maintain the solution free of CO. Then the Faradaic and ionic currents of $m/z = 44$ (CO_2) were recorded simultaneously by scanning the potential from 0.06 V up to 1.6 V vs. RHE at 10 mV s^{-1} and a constant flow of 5 μL s^{-1}. $K^*(CO_2)$ can be calculated according to Eq. (6) [22–25]:

$$K_{CO_2}^* = \frac{z \cdot Q_i^{CO_2}}{0.8 \cdot Q_F^{total}} \quad (6)$$

where, $Q_i^{CO_2}$ and Q_F^{total} are the ionic and total Faradaic charges corresponding to the formation of CO_2 respectively. The total Faradaic charge was corrected by a factor of 0.8 corresponding to 20% caused by double layer charging [26–28] due to non-faradaic charges related to the adsorption of sulfate, hydrogensulfate and hydroxide anions on Pt surface. Furthermore, *z* is the number of electrons involved in the oxidation of CO at Pt ($z = 2$) by means of Eq. (7), and assuming that the charge integration of the ionic current $m/z = 44$ is equal to the charge of the Faradaic current of $m/z = 44$ since the electrochemical oxidation of adsorbed CO is the only reaction at this applied potentials on Pt.

$$CO + H_2O \rightarrow CO_2 + 2H^+ + 2e^- \quad (7)$$

The calibration constants for N-volatile species such as NO and NO_2 cannot be determined experimentally. However, by taking into account the fragmentation patterns and the ionization probabilities, these constants can be roughly estimated using the calibration

Table 1
Chemical structure and characteristics of selected model compounds.

Chemical name	Chemical Structure	Chemical formula	M/g mol^{-1}
Benzoic acid	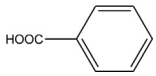	$C_7O_2H_6$	122.12
4-Nitrobenzoic acid	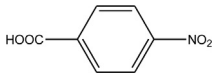	$C_7O_4NH_5$	167.12
4-Aminobenzoic acid	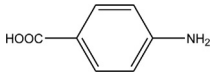	$C_7O_2NH_7$	137.14
4-Methylaminobenzoic acid	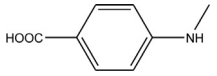	$C_8O_2NH_9$	151.16
4- Dimethylaminobenzoic acid	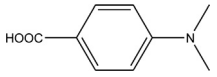	$C_9O_2NH_{11}$	165.19

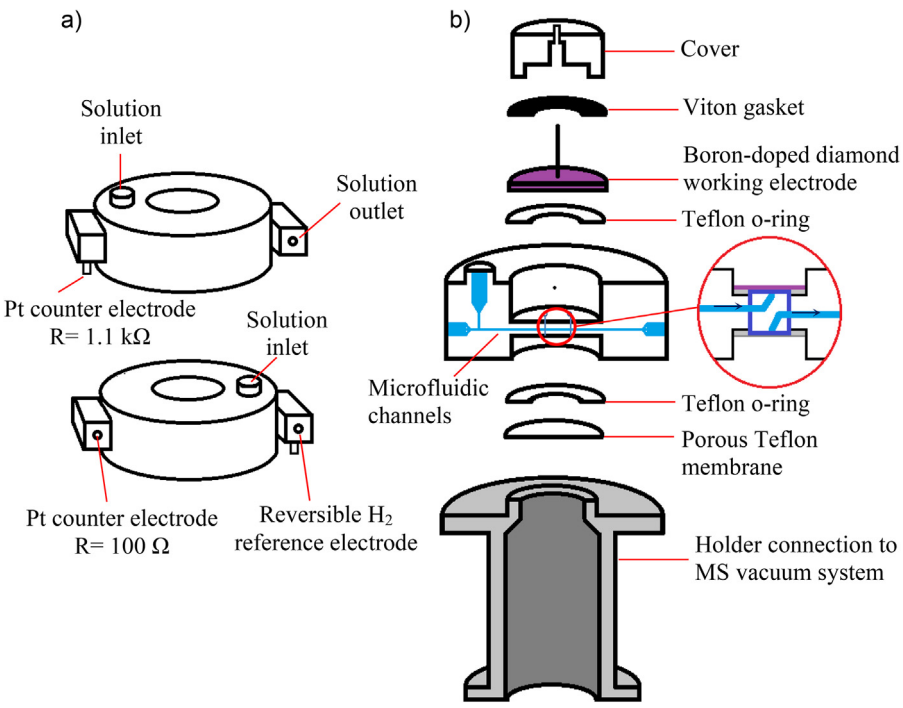

Fig. 1. Scheme of differential mass spectroscopy dual thin layer flow through cell.

constant of CO_2 [25,29]. Relative to N_2, the tabulated values of *IP* for NO = 1.2 while that of CO_2 = 1.4 for 100 eV electrode energy [30]. Assuming a very close molecular volume of CO_2 and NO_2, their relative ionization probabilities should be close. From this information, the calibration constants of NO and NO_2 can be calculated as follows:

$$K_i^* = K_{CO_2}^* \cdot \frac{IP_i}{IP_{CO_2}} \quad (8)$$

where, IP_i and IP_{CO_2} are the relative ionization probabilities of the *i* volatile species and CO_2, respectively.

Adsorbate coverage data of the amino compounds on BDD anode were calculated from the oxidation charge, assuming complete oxidation of the possibly formed adsorbate layers according to:

$$\theta = \frac{Q_F^{ad}}{z \cdot Q_F^{max}} \quad (9)$$

where θ is the equivalent number of adsorbate layers, Q_F^{ad} is the faradaic charge that corresponds to the adsorbate oxidation observed by integration of the corresponding adsorbate oxidation peaks, Q_F^{max} is the theoretical faradaic charge necessary for the oxidation of a densely packed monolayer [31].

3. Results and discussion

3.1. Evaluating the release of N-volatile species formed by hydroxyl radical oxidation

The conventional cyclic voltammogram (CV) at 10 mV s^{-1} from 0 up to 3.0 V and the mass spectrometric cyclic voltammograms (MSCV) for the volatile species of interest CO_2 (m/z = 44), NO (m/z = 30) and NO_2 (m/z = 46) were simultaneously recorded during the electrochemical analysis by means of DEMS. Two blank assays

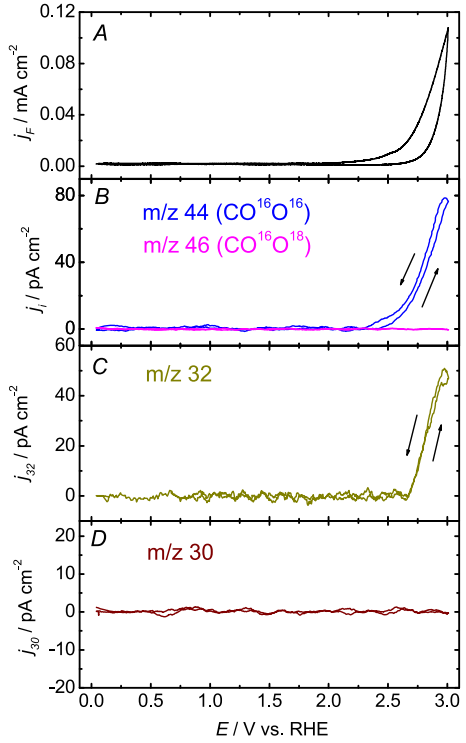

Fig. 2. Simultaneously recorded (a) CV and (b–e) MSCV of 1.0 M $NaClO_4$ at pH = 7 with BDD electrode at scan rate of 10 mV s^{-1} under constant flow rate of 5 μL s^{-1}. The MSCV were recorded for (b) CO_2 m/z = 44 and isotopic $CO^{16}O^{18}$ m/z = 46, (c) O_2 m/z = 32 and (d) NO m/z = 30.

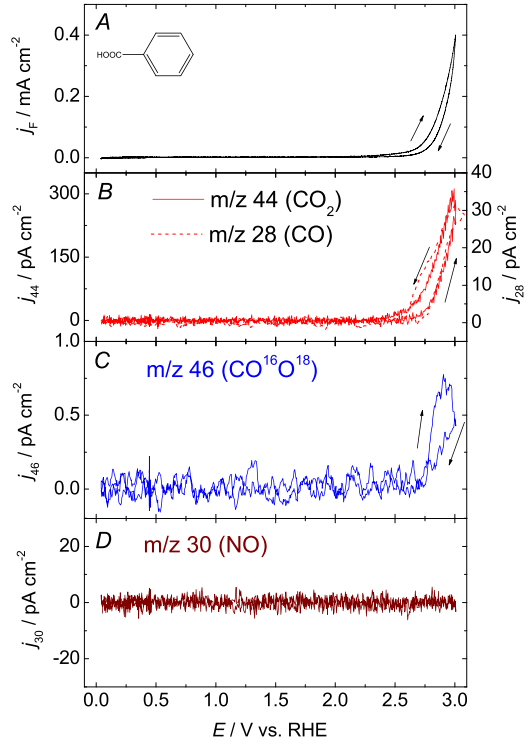

Fig. 3. Simultaneously recorded (a) CV and (b–e) MSCV during the oxidation with BDD of 10 mM of benzoic acid with 1.0 M $NaClO_4$ and pH = 7 at scan rate of 10 mV s^{-1} under constant flow rate of 5 μL s^{-1}. The MSCV were recorded for (b) CO_2 m/z = 44 and CO as fragment of CO_2 m/z = 28, (c) NO_2 m/z = 46 and (d) NO m/z = 30.

were carried out to ascertain the release of N-volatile species from the oxidation via •OH radical of N-containing organic pollutants.

The first blank analysis depicted in Fig. 2 corresponds to the electrochemical oxidation of a solution containing solely 1.0 M $NaClO_4$ as supporting electrolyte at neutral pH 7.0. The CV presents the usual shape of BDD voltammograms with a wide electrochemical window until water oxidation Reaction (1) at 2.5 V vs RHE, which results in the observed increase in the faradaic current density (Fig. 1a). As expected, N-volatile species were not detected due to the absence of any N source. On the other hand, noteworthy is the detection of CO_2 with low ionic current density of ca. 80 pA cm^{-2} and O_2 with ca. 50 pA cm^{-2}. The evolution of CO_2 could be justified from the corrosion of non-diamond sp^2 carbon impurities present in BDD anodes [32,33], as given by expression (10). On the other hand, the evolution of O_2 results from the recombination of •OH according to Reaction (11). Noteworthy is that oxygen evolution has not been detected in presence of organics since the mineralization process consumes preferentially the electrogenerated •OH thus suppressing the recombination reaction.

$$C(sp^2) + 2\,H_2O \rightarrow CO_2 + 4H^+ + 4\,e^- \quad (10)$$

$$2^{\bullet}OH \rightarrow O_2 + 2H^+ + 2\,e^- \quad (11)$$

Fig. 3 shows the DEMS analysis of the electrochemical oxidation of 10 mM benzoic acid with 1.0 M $NaClO_4$ at pH 7.0. Benzoic acid was selected as blank compound for these analyses since it presents the same molecular structure like all the N-containing compounds studied without any nitrogen functional group (see Table 1). Despite of presenting a similar-shape CV in Fig. 3 to the previous blank of Fig. 2, the higher faradaic current density (j_F) should be highlighted attaining of 0.4 mA cm^{-2} at 3.0 V vs. RHE, which corresponds to a 4-fold increase in comparison to the 0.1 mA cm^{-2} of the blank in absence of organics. This trend could be explained by the contribution of oxidation of intermediates or by-products involving direct charge transfer processes after the first oxidation by •OH radicals, which occurs in parallel to further •OH attacks. Despite of that contribution, the overall mineralization to CO_2 takes place only by the mediation of the •OH. From the increase in the ionic current density of m/z = 44 (j_{44}) which corresponds to CO_2 mass, it is obvious that the mineralization of benzoic acid is achieved only at higher potentials due to the action of the •OH radical. Similar to the MSCV in absence of organics, no signal corresponding to N-volatile species was expected on the oxidation of benzoic acid. However, a small current of 0.75 pA cm^{-2} was observed for m/z = 46 (j_{46}). This signal is of high relevance because it is not only produced by NO_2 but also by CO_2 due to the isotopic O^{18} ($CO^{16}O^{18}$ = 46). Thus, from the integration of the charge of the ionic currents of m/z = 44 ($CO^{16}O^{16}$) and m/z = 46 ($CO^{16}O^{18}$) of benzoic acid we can estimate a correction factor to subtract the isotopic contribution of the isotopic O^{18} in CO_2 from the actual signal that will correspond also to NO_2 in the following experiments. From the experimental results, the charge integrated from the isotopic CO_2 ionic current density is 0.003 times the charge of the CO_2 ionic current density for m/z = 44. This is close to the natural isotopic distribution in nature (0.4%); therefore the following correction factor expressed in Eq. (12) was used to discriminate the contribution of NO_2 on the ionic current densities of m/z = 46.

$$j_{46}^{NO_2} = j_{46}^{total} - 0.003 j_{44}^{total} \quad (12)$$

The evolution of volatile N-species during •OH mineralization of N-containing organic pollutants (compounds containing amino and nitro groups) as observed by DEMS is shown in Figs. 4–7 . These results demonstrate the feasible formation of NO_x species from the treatment of N-containing pollutants by AOPs based on the formation of highly oxidant species such as •OH [17]. The formation of NO_x has been hypothetically considered to explain the diminution of total nitrogen in solution during AOPs water treatments, but this is here for the first time being demonstrated and supported by

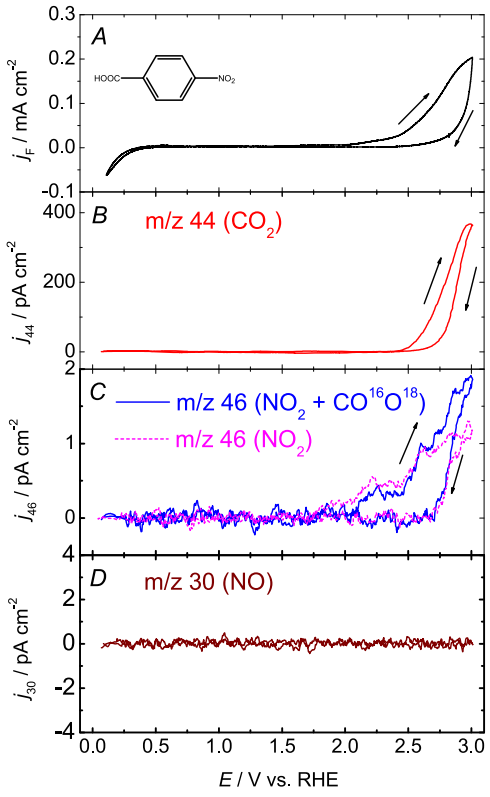

Fig. 4. Simultaneously recorded (a) CV and (b–e) MSCV during the oxidation with BDD of 10 mM of 4-nitrobenzoic acid with 1.0 M $NaClO_4$ and pH = 7 at scan rate of 10 mV s^{-1} under constant flow rate of 5 μL s^{-1}. The MSCV were recorded for (b) CO_2 m/z = 44, (c) NO_2 m/z = 46 and (d) NO m/z = 30.

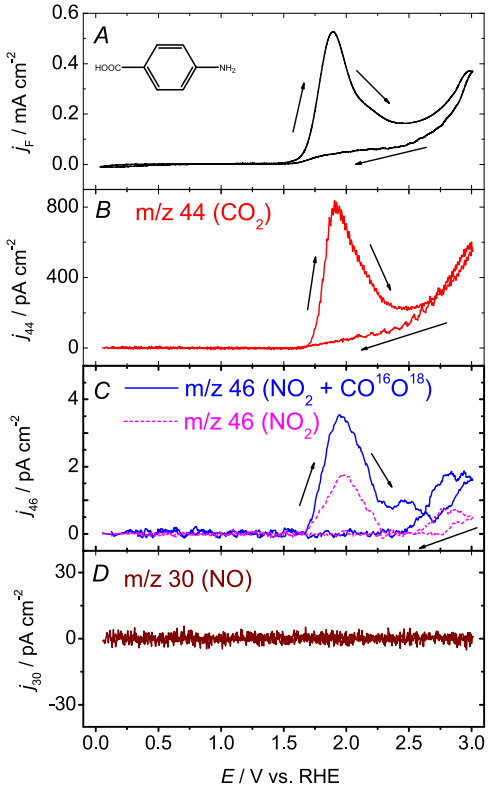

Fig. 5. Simultaneously recorded (a) CV and (b–e) MSCV during the oxidation with BDD of 10 mM of 4-aminobenzoic acid with 1.0 M $NaClO_4$ and pH = 7 at scan rate of 10 mV s^{-1} under constant flow rate of 5 μL s^{-1}. The MSCV were recorded for (b) CO_2 m/z = 44, (c) NO_2 m/z = 46 and (d) NO m/z = 30.

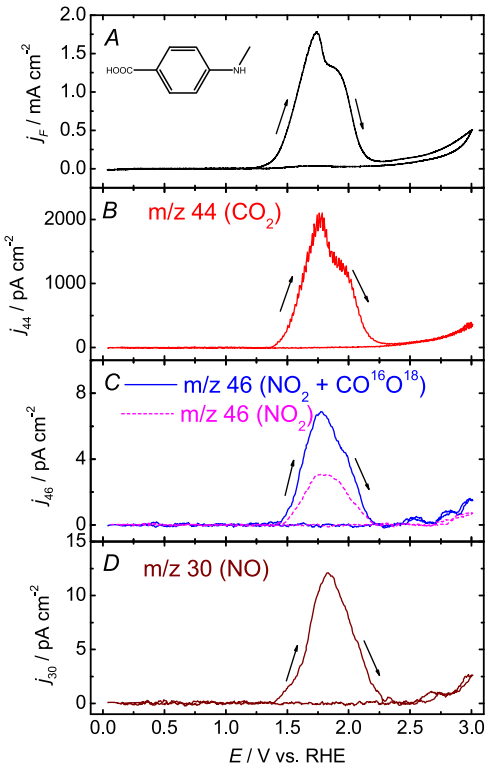

Fig. 6. Simultaneously recorded (a) CV and (b–e) MSCV during the oxidation with BDD of 10 mM of 4-methylaminobenzoic acid with 1.0 M $NaClO_4$ and pH = 7 at scan rate of 10 mV s^{-1} under constant flow rate of 5 μL s^{-1}. The MSCV were recorded for (b) CO_2 m/z = 44, (c) NO_2 m/z = 46 and (d) NO m/z = 30.

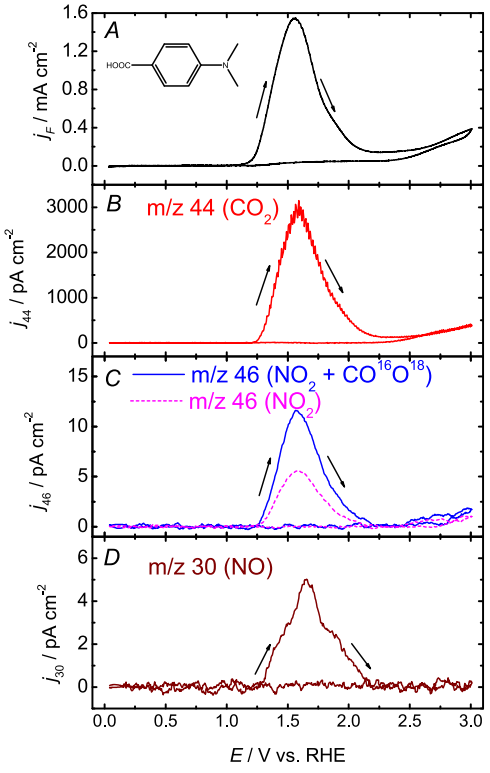

Fig. 7. Simultaneously recorded (a) CV and (b–e) MSCV during the oxidation with BDD of 10 mM of 4-dimethylaminobenzoic acid with 1.0 M $NaClO_4$ and pH = 7 at scan rate of 10 mV s^{-1} under constant flow rate of 5 μL s^{-1}. The MSCV were recorded for (b) CO_2 m/z = 44, (c) NO_2 m/z = 46 and (d) NO m/z = 30.

experimental results [8,12,14,16]. The particularities and species released from the treatment of each compound will be discussed thoroughly in the subsection below, since those are directly related to the nature of the nitrogenized functional group. However, it is important to remark that in any case the evolution of N_2 ($m/z = 28$) has not been observed. In all cases the quantified peaks of ($m/z = 28$) corresponds solely to the natural fragmentation of CO_2 as CO giving a signal equivalent to the 10% of the j_{44} according to the theoretical data bases and the experimental results obtained from the benzoic acid blank (see Fig. 3), the formation of N_2 not being discernible; and if it is formed, its amount is completely negligible. Notwithstanding, the formation of a N≡N triple bond from the oxidation of amino and nitro groups at mg dm^{-3} concentration by means of •OH is rarely expected.

3.2. Functional groups influence on the distribution of N-volatile species

As could be deduced from Figs. 4–7, the pollutants present different behavior and release different N-volatile species according to the nature of their nitrogenized functional group. From the mineralization of 4-nitrobenzoic acid (data collected in Fig. 4) we observe a flat CV with an increase in the faradaic current density at similar potentials vs. RHE as in the blank solutions. Noticeable is the lower faradaic current density achieved in comparison to the benzoic acid, due to the higher recalcitrant character (lower overall oxidation state) induced by the nitro substituent in the position C-4 that reduces the extent of the electrochemical charge transfer processes and consequently the j response during the potential sweep. Noticeable is also the lower onset potential and the hysteresis. Nevertheless, mineralization is attained in the potential range where •OH is electrogenerated and released from the oxygen terminated BDD surface as proved by the detection of high ionic current densities of CO_2 by mass spectroscopy. The ion current for CO_2 (cf. Fig. 4) is somewhat larger than in the case of benzoic acid, as expected from the higher overall oxidation state. The detailed analysis of N-volatile species by MSCV exhibits the mere evolution of NO_2. In fact, the formation of NO from the nitrogen of the former nitro group, which is in the higher oxidation state, only can be produced by reduction processes [34] that are absolutely unexpected in a highly oxidizing system of •OH radical.

On the other hand, special attention should be drawn to the voltammograms of amino-compounds studied and to the different species released by primary, secondary and tertiary amines according to MSCV analyses. As shown in Fig. 5, the CV of 4-aminobenzoic acid displays a peak of oxidation at 2.0 V vs. RHE at the forward potential sweep scan. A similar trend is observed in the CVs of 4-methylaminobenzoic acid and 4-dimethylaminobenzoic acid with peaks at 1.7 V and 1.6 V, respectively, shown in Figs. 6 and 7. The higher current densities recorded in the CV of the latter compounds could be related to the electron donor effect of the methyl substituents in the amino group favoring the charge transfer kinetics. Nonetheless, these peaks in all three amines are indicative of the oxidation of amino-compounds onto the BDD surface by direct charge transfer processes. The occurrence of the peak suggests that this is a surface limited process: the free pair of electrons of amino functional group is susceptible to interact with the surface of BDD leading competitively to adsorbed amino-organics terminated BDD surfaces at low potentials [19,35–37]. The integrated adsorbate oxidation Faradaic charges together with their equivalent coverages calculated for the primary, secondary and tertiary amino compounds are listed in Table 2. Noteworthy is that if the peaks are considered to correspond to an adsorbate oxidation, the high adsorbate charges suggest the formation of 20 or more monolayers of the adsorbate on the surface of the BDD at low potentials (assuming a packing density similar to that of a benzene monolayer on Pt [31] and complete oxidation to CO_2).

Table 2
Calculated peak oxidation faradaic charge (Q_F^{ad}) for the amino compounds at BDD surface together with their equivalent coverages (θ) assuming complete mineralization to CO_2 (cf. Eqs. (16)–(18), with z = 28 for 4-aminobenzoic acid, 34 for 4-methylaminobenzoic acid, and 40 for 4-dimethylamino benzoic acid) and assuming a packing density of a monolayer similar to that of benzene on Pt (0.3 nmol/cm^2) [31].

Chemical name	Q_F^{ad}/mC cm^{-2}	Θ/monolayers
4-Aminobenzoic acid	17.8	21
4-Methylaminobenzoic acid	68.7	70
4- Dimethylaminobenzoic acid	64.3	55

Moreover, the MSCV recorded at $m/z = 44$ (CO_2) indicates that the electrochemical charge transfer is related to a mineralization process due to the release of CO_2 which could be associated with the promotion of the decarboxylation reaction of adsorbed amines and demethylation reactions of the secondary and tertiary amines, as will be discussed subsequently. Similar peaks during the oxidation of N-containing organics on BDD anodes have been previously reported in the literature by Fujishima et al. [38,39] oxidizing aniline and Herold et al. [40] oxidizing pyridine. The authors suggested that these oxidation peaks correspond to a polymerization reaction of the aniline by the amine-imide conversion of the amino group, although polyaniline films where not observed on the BDD surface [38]. According to Fujishima et al. [38,39], the polymerization reaction could be a feasible reaction associated to the observed peak during the oxidation of the amino compounds studied. However, the DEMS analysis demonstrates the release of CO_2 associated to the peak oxidation as indicative of an alternative polymerization route. A possible explanation for the detection of CO_2 could be the electrochemical decarboxylation according to Kolbe Reaction (13), where the R• radical species can polymerize following a cascade reaction.

$$RCOO^- + e^- \rightarrow R^\bullet + CO_2 \quad (13)$$

The fact that only the amino benzoic acids are oxidized in a peak below 2 V suggests that the first step is a direct electron transfer from the amino group, which is followed by either the Kolbe reaction of an intermediate or some other oxidation reaction leading to CO_2. The number of electrons per formed CO_2 molecules is around 4–5 (cf. Table 3), which also shows that the Kolbe reaction is not the only reaction occurring in this potential range. It is important to remark the noticeable reduction of these peaks, which appear only as a shoulder on the backward CV sweep. This trend suggests that at high potentials the release of highly oxidant •OH near to the BDD surface from the oxygen termination mineralizes all the organics diffused to the anode surface [36,37]. Thereby, the oxygen termination of BDD at high potentials could explain the considerable reduction of the backwards oxidation peak; further research is necessary to really understand these peaks. Nonetheless, apart from the oxidation by direct charge transfer reactions of these amino pollutants, similar to other organic species they are oxidized by •OH at applied potentials over 2.5 V vs. RHE.

A further analysis on the N-volatile species released by MSCV highlights the appreciable differences depending on the subcategory of the amino group of the pollutant oxidized by •OH. As can be seen from Fig. 5, only NO_2 is released from the degradation of 4-aminobenzoic by means of •OH. According to the general degradation pathways of aromatic primary amines, the preferential attack of the non-selective •OH occurs on the more nucleophilic C-4 position due to the electronegative character of the nitrogen substituent yielding ammonium cation (NH_4^+) [8,12]. However, from the MSCV the release of NO_2 was ascertained. The release of this noxious volatile species could contribute to explain the loss of

Table 3
Calculated current efficiencies for the release of CO_2, NO_2 and NO during the mineralization of organic pollutants and number of electrons z per formed CO_2.

Compounds	Assumed nitrogen product	% CE (CO_2)	% CE (NO_2)	% CE (NO)	Experimental z values	Theoretical z values
Benzoic acid	–	80	–	–	5.4	4.3
4-Nit robenzoic acid	NO_3^-	94		–	3.4	3.1
	NO_2	124	4.7			4.1
4-Aminobenzoic acid	NH_4^+	86			4.6 (3.7)	4.0
	NO_2	108	0.6	–		5.0
4-Methyl-amino-	NH_4^+	51			8.0 (5.2)	4.3
benzoic	NO_2	61	0.5			5.1
acid	NO	58		2.4		4.9
4-Dimethyl-amino-	NH_4^+	71			5.2 (3.5)	4.3
benzoic	NO_2	86	1.3			5.2
acid	NO	82		1.0		5.0

z values in brackets refer to the low potential region (4-Aminobenzoic acid: 1.5–2.5 V, 4-Methyl-aminobenzoic acid and 4-Dimethylaminobenzoic acid: 1.25–2.25 V vs. Ag/AgCl). Other z values refer to the high potential region (Benzoic acid: 2.25–3 V, 4-Nitrobenzoic acid: 2–3 V, 4-Aminobenzoic acid: 2.5–3 V, 4-Methyl-amino-benzoic acid and 4-Dimethylaminobenzoic acid: 2.25–3 V vs. Ag/AgCl).

nitrogen in the mass balance during AOPs oxidation of N-containing pollutants. The main difference with 4-nitrobenzoic acid is that this species has been detected not only at high potentials but also on the oxidation peak of adsorbed 4-aminobenzoic acid. The oxidation of amines to amine oxides with H_2O_2, MnO_4^- or other oxidants where nitrogen atom acts as nucleophile is well known [41,42], being its oxidation by •OH assumable as could be deduced from the identification of nitrates during amino compounds oxidation [12,16,17,43].

The mineralization of 4-methylaminobenzoic acid in Fig. 6 shows the preferential release of NO as volatile species followed by its further oxidation as NO_2. Similarly to 4-aminobenzoic acid, these NO_x species are identified from the direct charge transfer reaction at 1.7 V vs. RHE on the nitrogen terminated BDD and the •OH at higher applied potentials. The formation of NO could be explained by the demethylation step required previous to the release of NOx species by the attack of •OH [43]. Analogous behavior is observed on the mineralization of the tertiary amine and the 4-dimethylaminobenzoic acid shown in Fig. 7. However, the amount of NO released diminishes since the loss of both methyl alkyl substituents leads preferentially to the most oxidized form as NO_2 due to the requirement of two •OH attack to remove both methylene substituents.

3.3. Estimation of the current efficiency on the generation of NOx species by electrogenerated •OH

The MSCV results discussed on the mineralization of N-containing aromatic pollutants by •OH demonstrate qualitatively, for the first time, the release of these noxious species from EO water treatment technologies. However, from the current efficiency (CE) for the generation of each species, the amount of N-volatiles evolved can be semi-quantitatively estimated with respect to CO_2 evolved from mineralization process.

The number of electrons required to mineralize benzoic acid is given by Eq. (14). Nonetheless, it is important to remark that the overall mineralization reaction of each compound and the required electrons will depend on the nitrogen species released. It is important to remark that different pathways can coexist simultaneously being one of them preferred, therefore the different overall mineralization reactions conducting to the different ionic and N-volatile species will be described subsequently. The number of moles of electrons required per mol of CO_2 for each compound was estimated considering the main nitrogen species depending on the functional group according to literature of N-compounds oxidation. Then, nitrate was considered the main by-product of 4-nitrobenzoic acid mineralization by •OH [15,44] following Eq. (15). Whereas, it has been considered that the amines oxidation by •OH leads as main product ammonium ion [8,12] according Reactions (16) for 4-aminobenzoic acid, (17) for 4-methylaminobenzoic acid and (18) for 4-dimethylbenzoic acid.

$$C_7O_2H_6 + 12\,H_2O \rightarrow 7\,CO_2 + 30\,H^+ + 30\,e^- \quad (14)$$

$$C_7O_4NH_5 + 13\,H_2O \rightarrow 7\,CO_2 + NO_3^- + 31\,H^+ + 30\,e^- \quad (15)$$

$$C_7O_2NH_7 + 12\,H_2O \rightarrow 7\,CO_2 + NH_4^+ + 27\,H^+ + 28\,e- \quad (16)$$

$$C_8O_2NH_9 + 14\,H_2O \rightarrow 8\,CO_2 + NH_4^+ + 33\,H^+ + 34\,e^- \quad (17)$$

$$C_9O_2NH_{11} + 16\,H_2O \rightarrow 9\,CO_2 + NH_4^+ + 39\,H^+ + 40\,e^- \quad (18)$$

This corresponds to 4.3 mol e^-/mol CO_2 for benzoic acid, 4.3 mol e^-/mol CO_2 for 4-nitrobenzoic acid, 4.0 mol e^-/mol CO_2 for 4-aminobenzoic acid, 4.3 mol e^-/mol CO_2 for 4-methylbenzoic acid, and 4.4 mol e^-/mol CO_2 for 4-dimethylbenzoic acid, respectively.

On the other hand, in order to determine the number of electrons consumed on the release of each N-volatile species different overall mineralization should be considered. According to the experimental results, the corresponding equation of each pollutant for the release of NO_x species will be stated accordingly. Then, the general expressions to the release of NO_2 observed in all of the N-containing aromatics are described by the following Eqs. (19)–(22):

$$C_7O_4NH_5 + 12\,H_2O \rightarrow 7\,CO_2 + NO_2 + 29\,H^+ + 29\,e^- \quad (19)$$

$$C_7O_2NH_7 + 14\,H_2O \rightarrow 7\,CO_2 + NO_2 + 35\,H^+ + 35\,e^- \quad (20)$$

$$C_8O_2NH_9 + 16\,H_2O \rightarrow 8\,CO_2 + NO_2 + 41\,H^+ + 41\,e- \quad (21)$$

$$C_9O_2NH_{11} + 18\,H_2O \rightarrow 9\,CO_2 + NO_2 + 47\,H^+ + 47\,e^- \quad (22)$$

where 29 mol e^- for 4-nitrobenzoic acid, 35 mol e^- for 4-aminobenzoic acid, 41 mol e^- for 4-methylbenzoic acid and 47 mol e^- for 4-dimethylbenzoic acid are required for the release of 1 mol of NO_2, respectively.

The number of electrons to yield 1 mol of NO by 4-methylaminobenzoic acid of 39 and by 4-dimethylaminobenzoic acid of 45 were determined according to Eqs. (23) and (24), respectively.

$$C_8O_2NH_9 + 15\,H_2O \rightarrow 8\,CO_2 + NO + 39\,H^+ + 39\,e^- \quad (23)$$

$$C_9O_2NH_{11} + 17\,H_2O \rightarrow 9\,CO_2 + NO + 45\,H^+ + 45\,e^- \quad (24)$$

In Table 3 the calculated current efficiencies for the generation of each volatile species from the mineralization of each organic compound by *in situ* electrogenerated •OH are collected together with the calculated number of electrons per formed CO_2 molecule. The latter number is higher in the high potential range than at potentials where the peak is observed due to the more complete combustion. The results evidence high efficiencies in the range of 50 up to 86% of

efficiency on the evolution of CO_2 that reveal that the current circulated is mainly used to mineralize the organic pollutants that reach the anode surface, whereas low efficiencies on the release of N-volatiles were estimated. This result agrees with the preferred yield of ionic nitrogen species reported in literature, mainly NH_4^+ and NO_3^- [8–18,20]. However, it demonstrates that the loss of nitrogen observed in the mass balances could be attributed in some extent to the formation of NO_x by •OH.

A rough calculation allows estimating that from 140 mg dm^{-3} of initial N (content in 10 mM of each pollutant) 6.6 mg dm^{-3} of N, 0.81 mg dm^{-3} of N, 0.66 mg dm^{-3} of N and 1.84 mg dm^{-3} of N could be lost as NO_2 from 4-nitrobenzoic acid, 4-aminobenzoic acid, 4-methylaminobenzoic acid and 4-dimethylaminobenzoic acid by their mineralization by •OH. Moreover, 5.18 mg dm^{-3} of N and 1.50 mg dm^{-3} of N were lost as NO from 4-methylaminobenzoic and 4-dimethylaminobenzoic acids oxidation. These experiments were carried out with model pollutants concentrations of 10 mM (ca. 1 g dm^{-3}) in order to determine effectively the concentrations of the NO_x generated. However, it should be taken into account that persistent and emerging pollutants concentrations in water are in the range of μg dm^{-3} and ng dm^{-3} [1–3]. Thereby, from these results the amount of noxious NO_x species released from AOPs actual treatment of wastewaters polluted with N-containing organic compounds with amino and nitro functional groups is expected to be approximately of three orders of magnitude lower than the concentration of nitrogen in the pollutant, which supposes concentrations of ng dm^{-3}. The release of NO_2 is limited by the European Commission by law to not exceed average values of 40 μg m^{-3}, where peak concentrations cannot be above 200 μg m^{-3} per hour [45], as it is recommended by the World Health Organization [46]. In conclusion, the low amounts of NO_x released from •OH oxidation of N-containing organics cannot be considered hazardous. Thus, AOPs could still be considered promising environmental-friendly technologies to efficiently decontaminate wastewaters containing organic pollutants.

4. Conclusions

DEMS analysis allowed demonstrating experimentally the release of NO_x species during organic pollutants mineralization by •OH radicals. The systematic study of model organic compounds containing organic nitrogen has provided valuable information on the relationship between NO_x species released with the nitrogenized functional groups. Thereby, while only NO_2 has been detected from the primary amino group and the nitro group, NO was evolved from secondary and tertiary amines during the demethylation reaction. The quantification of released species from the current efficiencies highlighted the low extent of NO_x species evolved from the •OH oxidation of amino and nitro functional groups, which are ca. three orders of magnitude lower than the initial dissolved organic nitrogen in solution. Taking into account that persistent organic pollutants and contaminants of emerging concern are found in water effluents in concentrations ranged between μg dm^{-3} and ng dm^{-3}, the expected release of these noxious volatile nitrogen species from AOPs water treatment technologies are far from hazardous concentrations stated by law of 40 μg m^{-3}. Thus, despite of NO_x species being released, the EO with BDD anodes can still be considered an environmental friendly alternative to depollute wastewaters containing organic pollutants. Since the main oxidant involved in the mineralization process is the electrogenerated •OH radical, these results suggest that similar trends could be expected for other AOPs, although experimental evidences should be reported for each process.

Acknowledgments

Dr. Garcia-Segura acknowledges the financial support from Green Talents award from Forschung für Nachhaltige Entwicklung of Bundesministerium für Bildung und Forschung of the German Federal Government. The authors highly appreciate the kindly suggestions and supports given by Dr. S. Ernst and Dr. A.A. Abd-El-Latif.

References

[1] T. Ternes, A. Joss, J. Oehlmann, Occurrence fate, removal and assessment of emerging contaminants in water in the water cycle (from wastewater to drinking water), Water Res. 72 (2015) 1–2.
[2] B. Chen, Y. Kim, P. Westerhoff, Ocurrence and treatment of wastewater-derived organic nitrogen, Water Res. 45 (2011) 4641–4650.
[3] N. Collado, S. Rodriguez-Mozaz, M. Gros, A. Rubirola, D. Barceló, J. Comas, I. Roriguez-Roda, G. Buttiglieri, Pharmaceuticals occurrence in a WWTP with significant industrial contribution and its input into the river system, Environ. Pollut. 185 (2014) 202–212.
[4] C. Prasse, D. Stalter, U. Schulte-Oehlmann, J. Oehlmann, T.A. Ternes, Spoilt for choice: a critical review on the chemical and biological assessment of current wastewater treatment technologies, Water Res. 87 (2015) 237–270.
[5] E. Brillas, I. Sirés, M.A. Oturan, Electro-Fenton process and related electrochemical technologies based on Fenton's reaction chemistry, Chem. Rev. 109 (2016) 6570–6631.
[6] R. Fagan, D.E. McCormack, D.D. Dionysiou, S.C. Pillai, A review of solar and visible light active TiO_2 photocatalysis for treating bacteria: cyanotoxins and contaminants of emerging concern, Mater. Sci. Semicon. Proc. 42 (2016) 2–14.
[7] C.A. Martínez-Huitle, M.A. Rodrigo, I. Sirés, O. Scialdone, Single and coupled electrochemical processes and reactors for the abatement of organic wáter pollutants: a critical review, Chem. Rev. 115 (2015) 13362–13407.
[8] I. Nitoi, P. Oancea, I. Cristea, L. Constsntin, G. Nechifor, Kinetic and mechanism of chlorinated aniline degradation by TiO2 photocatalysis, J. Photochem. Photobiol. A 298 (2015) 17–23.
[9] G. Perchet, G. Merlina, J.-C. Revel, M. Hafidi, C. Richard, E. Pinelli, Evaluation of a TiO2 photocatalysis treatment on nitrophenols and nitramines contaminated plant wastewaters by solid-phase extraction coupled with ESI PLC-MS, J. Hazard. Mater. 166 (2009) 284–290.
[10] A. Tekle-Röttering, C. von Sonntag, E. Reisz, C. vom Eyser, H.V. Lutze, J. Türk, S. Naumov, W. Schmidt, Ozonation of anilines: kinetics stoichiometry, product identification and elucidation of pathways, Water Res. 98 (2016) 147–159.
[11] A. Tekle-Röttering, E. Reisz, K.S. Jewell, H.V. Lutze, T.A. Ternes, W. Schmidt, T.C. Schmidt, Ozonation of pyridine and other N-heterocyclic aromatic compounds: kinetics stoichiometry, identification of products and elucidation of pathways, Water Res. 102 (2016) 582–593.
[12] A. Serra, X. Domènech, C. Arias, E. Brillas, J. Peral, Oxidation of α-methylphenylglycine under Fenton and electro-Fenton conditions in the dark and in the presence of solar light, Appl. Catal. B: Environ. 89 (2009) 12–21.
[13] N. Masomboon, C. Ratanatamskul, M.-C. Lu, Kinetics of 2,6-dimethylaniline oxidation by various Fenton processes, J. Hazard. Mater. 192 (2011) 347–353.
[14] A. Thiam, I. Sirés, J.A. Garrido, R.M. Rodríguez, E. Brillas, Decolorization and mineralization of Allura Red AC aqueous solutions by electrochemical advanced oxidation processes, J. Hazard. Mater. 290 (2015) 34–42.
[15] T. Pérez, S. Garcia-Segura, A. El-Ghenymy, J.L. Nava, E. Brillas, Solar photoelectro-Fenton degradation of the antibiotic metronidazole using a flow plant with a Pt/air-diffusion cell and a CPC photoreactor, Electrochim. Acta 165 (2015) 173–181.
[16] M.J.M. de Vidales, M. Millán, C. Sáez, P. Cañizares, M.A. Rodrigo, What happens to inorganic nitrogen species during conductive diamonds electrochemical oxidation of real wastewater? Electrochem. Commun. 67 (2016) 65–68.
[17] S. Garcia-Segura, E. Brillas, Mineralization of the recalcitrant oxalic and oxamic acids by electrochemical advanced oxidation processes using a boron-doped diamond anode, Water Res. 45 (2011) 2975–2984.
[18] E.B. Cavalcanti, S. Garcia-Segura, F. Centellas, E. Brillas, Electrochemical incineration of omeprazole in neutral aqueous medium using a platinum or boron-doped diamond anode. Degradation kinetics and oxidation products, Water Res. 47 (2013) 1803–1815.
[19] P.M. Quaino, W. Schmickler, Oxygen-terminated diamond electrodes in alkaline media: structure and OH generation, ChemElectroChem 1 (2014) 933–939.
[20] H. Rubí-Juárez, S. Cotillas, C. Sáez, P. Cañizares, C. Barrera-Díaz, M.A. Rodrigo, Removal of herbicide glyphosate by conductive-diamond electrchemical oxidation, Appl. Catal. B: Environ. 188 (2016) 305–312.
[21] I. Kisacik, A. Stefanova, S. Ernst, H. Baltruschat, Oxidation of carbon monoxide: hydrogen peroxide and water at a boron doped diamond electrode: the competition for hydroxyl radicals, Phys. Chem. Chem. Phys. 15 (2013) 4616–4624.
[22] A. Stefanova, S. Ayata, A. Erem, S. Ernst, H. Baltruschat, Mechanistic studies on boron-doped diamond: oxidation of small organic molecules, Electrochim. Acta 110 (2013) 560–569.
[23] A.A. Abd-El-Latif, C.J. Bondue, S. Ernst, M. Hegemann, J.K. Kaul, M. Khodayari, E. Mostafa, A. Stefanova, H. Baltruschat, Insights into electrochemical

reactions by differential electrochemical mass spectrometry, Trends Anal. Chem. 70 (2015) 4–13.
[24] A. Kapalka, B. Lanova, H. Baltruschat, G. Fóti, C. Comninellis, Electrochemically induced mineralization of organics by molecular oxygen on boron-doped diamond electrode, Electrochem. Commun. 10 (2008) 1215–1218.
[25] H. Baltruschat, Differential electrochemical mass spectroscopy, J. Am. Soc. Mass Spectrom. 15 (2004), 1963–1706.
[26] H. Baltruschat, U. Schmiemann, The adsorption of unsaturated organic species at single crystal electrodes studied by differential electrochemical mass spectrometry, Ber. Bunsenges. Phys. Chem. 97 (1993) 452–460.
[27] J. Willsau, J. Heitbaum, Analysis of adsorbed intermediates and determination of surface potential shifts by dems, Electrochim. Acta 31 (1986) 943–948.
[28] J. Clavilier, R. Albalat, R. Gómez, J.M. Orts, J.M. Feliu, A. Aldaz, Study of the charge displacement at constant potential during CO adsorption on Pt(110) and Pt(111) electrodes in contact with a perchloric acid solution, J. Electroanal. Chem. 330 (1992) 489–497.
[29] NIST Chemistry Webbook, 2003, Available from: http://webbook.nist.gov/chemistry.
[30] Quadrupole Mass Spectrometry, in: BalzersInstruments (Ed.), P.p.m.i.V. technology, 1998.
[31] U. Schmiemann, H. Baltruschat, The influence of the single-crystal orientation on the electrocatalytic hydrogenation of benzene and the H-D exchange, J. Electroanal. Chem. 347 (1993) 93–109.
[32] S. Garcia-Segura, E.V. dos Santos, C.A. Martínez-Huitle, Role of sp3/sp2 ratio on the electrocatalytic properties of boron-doped diamond electrodes: a mini review, Electrochem. Commun. 59 (2015) 52–55.
[33] A. Kapalka, B. Lanova, H. Baltruschat, G. Fóti, C. Comninellis, A DEMS study of methanol and formic acid oxidation on boron-doped diamond electrode, J. Electrochem. Soc. 156 (2009) E149–E153.
[34] D.J. Dixon, O.P. Morejón, Recent developments in the reduction of nitro and nitroso compounds, in: P. Knochel, G.A. Molander (Eds.), Comprehensive Organic Synthesis, Elsevier, Amsterdam, 2014, pp. 479–492.
[35] Y. Song, K. Larsson, A theoretical study of the effect of dopants on dimond (100) surface stabilization for different termination scenarios, J. Phys. Chem. C 119 (2015) 2545–2556.
[36] M.M. Hassan, K. Larsson, Effect of surface termination on diamond (100) surface electrochemistry, J. Phys. Chem. C 118 (2014) 22995–23002.
[37] Z. Futera, T. Watanabe, Y. Einaga, Y. Tateyama, Principles calculation study on surfaces and water interfaces of boron-doped diamonf, J. Phys. Chem. C 118 (2014) 22040–22052.
[38] M. Mitadera, N. Spataru, A. Fujishima, Electrochemical oxidation of aniline at boron-doped diamond electrodes, J. Appl. Electrochem. 34 (2004) 249–254.
[39] T. Spataru, N. Spataru, A. Fujishima, Detection of aniline at boron-doped diamond electrodes with cathodic stripping voltmmetry, Talanta 73 (2007) 404–406.
[40] S. Herold, S. Möhle, M. Zirbes, F. Richter, H. Nefzger, S.E. Waldvogel, Electrochemical amination of less-activated alkylated arenes using boron-doped diamond anodes, Eur. J. Org. Chem. (2016) 1274–1278.
[41] S.S. Rawalay, H. Shechter, Oxidation of primary, secondary, and tertiary amines with neutral permanganate. Simple method for degrading amines to aldehydes and ketones, J. Org. Chem. 32 (1967) 3129–3131.
[42] R.D. Bach, M.-D. Su, H.B. Schlegel, Oxidation of amines and sulfides with hydrogen peroxide and alkyl hydrogen peroxide. The nature of the oxygen-transfer step, J. Am. Chem. Soc. 116 (1994) 5379–5391.
[43] A. Manassero, C. Passalia, A.C. Negro, A.E. Cassano, C.S. Zalazar, Glyphosate degradation in water employing the H2O2/UVC process, Water Res. 44 (2010) 3875–3882.
[44] J. Zhou, J. Xiao, D. Xiao, Y. Guo, C. Fang, X. Lou, Z. Wang, J. Liu, Transformations of chloro and nitro groups during the peroxymonosulfate-based oxidation of 4-chloro-2-nitrophenol, Chemosphere 134 (2015) 446–451.
[45] http://ec.europa.eu/environment/air/quality/standards.htm.
[46] http://www.who.int/phe/health_topics/outdoorair/outdoorair_aqg/en/.